

Simulation of Parasitic Backward-Wave Excitation in High-Power Gyrotron Cavities

Konstantinos A. Avramidis¹, Alexander Marek², Ioannis Chelis¹, Zisis C. Ioannidis¹, *Member, IEEE*, Lukas Feuerstein², John Jelonnek², *Senior Member, IEEE*, Manfred Thumm², *Life Fellow, IEEE*, and Ioannis Tigelis¹, *Senior Member, IEEE*

Abstract—The possibility of parasitic excitation of backward waves directly in the gyrotron cavity is demonstrated, by simulation, for two existing high-power gyrotrons. These are the 140-GHz 1-MW TE_{28,8}-mode gyrotron for the stellarator W7-X and the 140-GHz 1.5-MW TE_{28,10}-mode gyrotron, also for W7-X. The parasitic backward waves, namely, the TE_{23,7} mode in the 1-MW gyrotron and the TE_{−24,10} mode in the 1.5-MW gyrotron, are excited at high frequencies (RF), which are of the order of ~10% lower than the nominal operating frequency and which can lead to significant performance degradation, with respect to the output power, efficiency, and stability of the tube. This finding offers an additional possibility, besides parasitic mode excitation in the gyrotron beam tunnel or after the gyrotron cavity, for the origin of experimentally observed RF parasitic oscillations in high-power, high-frequency gyrotrons, operating in high-order modes. To strengthen the confidence in the simulation, the results of two codes, each using different modeling of the interaction between the electron beam and the RF wave, are compared and the appropriateness of the modeling with respect to the accurate simulation of backward waves is discussed in detail.

Index Terms—Backward waves, gyrotron, gyrotron simulation.

I. INTRODUCTION

DURING the experimental testing of high-power gyrotrons, the detection of high-frequency (RF) parasitic

This work was supported by the EUROfusion Consortium funded by the Euro-pean Union via the Euratom Research and Training Program under Agreement 101052200—EUROfusion. Views and opinions expressed are however those of the author(s) only and do not necessarily reflect those of the European Union or the European Commission. Neither the European Union nor the European Commission can be held responsible for them. The review of this article was arranged by Editor J. Feng. (*Corresponding author: Konstantinos A. Avramidis.*)

Konstantinos A. Avramidis, Ioannis Chelis, and Ioannis Tigelis are with the Department of Physics, National and Kapodistrian University of Athens, 15784 Athens, Greece (e-mail: kavramidis@phys.uoa.gr).

Alexander Marek, Lukas Feuerstein, John Jelonnek, and Manfred Thumm are with the Institute for Pulsed Power and Microwave Technology, Karlsruhe Institute of Technology, 76131 Karlsruhe, Germany.

Zisis C. Ioannidis is with the Department of Aerospace Science and Technology, National and Kapodistrian University of Athens, Psachna Evias, 34400 Athens, Greece.

Color versions of one or more figures in this article are available at <https://doi.org/10.1109/TED.2023.3242216>.

oscillations, appearing at frequencies ~5%–15% lower than the nominal operating frequency, is not uncommon [1], [2], [3], [4], [5], [6], [7]. Such oscillations can be of major concern if they are excited at operating parameters close to nominal and hamper the desired operation of the tube in terms of stability, efficiency, and output power: there are cases where the drop in the tube performance, related to the onset of such parasitic oscillations, is quite significant and is the major undesired result of the appearance of the parasitic frequencies. In experiments, the RF parasitic oscillations are usually detected in the frequency spectrum of the radiation leaving the gyrotron from the microwave windows. Therefore, it is not straightforward to experimentally determine the exact position in the gyrotron, where these oscillations are excited.

By combining theoretical studies with experimental findings, the RF parasitic oscillations have been, as a rule, attributed to parasitic beam–wave interaction in the beam tunnel before the gyrotron cavity (e.g., [1], [2], [3], [4], [5]). In this case, the spread in the energy and velocity of the electron beam, induced by the parasitic interaction in the beam tunnel, results in a nonoptimal electron beam in the cavity, explaining the observed performance drop.

An alternative suggestion has been that RF parasitic oscillations, at the frequency range under discussion, can also be generated by interaction of the operating mode with the electron beam after the cavity, at the region of the uptaper and launcher. This interaction generates a frequency lower than the nominal, due to the decreased magnetostatic field at that region, and is referred to as dynamic after-cavity interaction [6], [7], [8], [9]. Of course, since the parasitic interaction does not directly affect the electron beam properties in the cavity, the impact of this kind of parasitic interaction on gyrotron performance is expected to be less severe compared to that of the beam-tunnel parasitics.

A third possibility with respect to the origin of RF parasitic oscillations in the frequency range ~5%–15% lower than the nominal frequency has been lately proposed in [10], where it has been suggested that the harmful parasitic frequencies can also originate from backward waves excited in the gyrotron cavity itself. It should be mentioned that excitation, in simulation, of a backward-wave parasitic mode at a frequency 4% lower than the nominal frequency was also seen in [11], for a 4-MW coaxial-cavity gyrotron design. In the present

work, this possibility of origin of RF parasitic oscillations is theoretically examined in detail, using the geometry and operating parameters of two existing high-power, continuous wave (CW) gyrotrons, namely, the 140-GHz 1-MW gyrotron for the stellarator Wendelstein 7-X (W7-X) [12], operating in the $TE_{28,8}$ mode with eigenvalue 60.1, and the 140-GHz 1.5-MW gyrotron for W7-X [13], operating in the $TE_{28,10}$ mode with eigenvalue 67.1. It is shown by simulation that, for typical values of the electron velocity ratio $\alpha = 1.2$ – 1.3 or a little higher, parasitic backward-wave excitation is possible in the gyrotron cavity, resulting in noticeable performance degradation of the gyrotron. It is also shown that the parasitic interaction can extend also into the spacer region, i.e., in the intermediate region between the cavity and the beam tunnel.

The possibility of parasitic mode excitation in the spacer was also investigated in [14] by a single-mode model, which examined separately the excitation of each candidate parasitic mode. However, with that method, it was not possible to conclude which parasitic modes would actually be excited in the presence of the nominal mode and the additional competing modes. In this article, the above limitation is overcome by multimode modeling of the full cavity and spacer region, addressing the competition between the nominal operating mode, the standard forward-wave gyrotron modes close to cutoff, and the possible backward-wave modes.

RF parasitic oscillations at frequencies lower than nominal may also be attributed to the well-known three-wave interaction effect (e.g., [15], [16]). In this case, the excitation of the operating TE_{mp} mode at high power is accompanied by the simultaneous excitation of the azimuthal satellite modes $TE_{(m-1)p}$ and $TE_{(m+1)p}$ at low power. However, as the order of the operating mode increases, the frequency difference between this mode and its lower azimuthal satellite becomes smaller. For example, if the eigenvalue of the TE_{mp} mode is of the order of 50, the frequency of the $TE_{(m-1)p}$ mode is only 2%–3% lower. Consequently, for gyrotrons operating in a high-order mode, as is the case for the 140-GHz gyrotrons considered here as well as for practically all the contemporary MW-class CW gyrotrons operating above 140 GHz, the three-wave interaction effect is not likely to explain experimentally observed parasitic frequencies that are $\sim 5\%$ – 15% lower than the nominal frequency.

It should also be noted that in most studies of mode competition in high-power, high-frequency gyrotrons (see, for example, [17] and references therein), only the modes with cutoff frequency close to the cyclotron frequency are considered as competing modes. This is because, in the standard gyrotron interaction regime, a mode is excited close to cutoff and the Doppler term in the cyclotron resonance condition $\omega - k_{\parallel}v_{\parallel} \cong \omega_{\text{cycl}}$ is neglected. In contrast to that, the parasitic modes investigated in this article are backward waves excited not so close to cutoff; therefore, the Doppler term is nonnegligible. This has two principal consequences: first, to reproduce the field profile of a backward wave, an interaction model assuming nonfixed axial field structure

(e.g., [18]), rather than a model assuming fixed field structure (e.g., [15], [16]), is necessary. Second, the competing mode list should also extend to modes with a cutoff frequency quite lower than the cyclotron frequency.

For the simulation of the interaction of the electron beam with the resonant TE modes in the cavity, two multimode, time-dependent codes are used. The first code is EURIDICE [19], which is based on the trajectory approach and uses a slow-variables, gyro-averaged model of interaction, similar to that of [18]. Still, EURIDICE incorporates some additional advanced features, in particular the improvements with respect to the reference frequencies described in [20] as well as the consideration of all components of the magnetostatic and the RF magnetic field. The second code is simpleRick [21], which also uses the slow-variables approach for the RF field, but it is a 3-D particle-in-cell (PIC) code as far as the electron motion is concerned, without resorting to gyro-averaging of the electron motion. It should be noted that the advances (with respect to the “standard” gyrotron interaction model of [18]) incorporated in EURIDICE and simpleRick are necessary for the correct modeling of the backward-wave excitation. This is discussed in detail in this work.

This article is organized as follows. In Section II, parasitic backward-wave excitation in the cavities of the two high-power gyrotrons for W7-X is demonstrated by multimode simulations with EURIDICE. The mechanism resulting in the performance degradation of the gyrotron is illustrated, and the influence of the electron velocity spread, which is a somewhat unknown quantity in experimental set-ups, is studied. In Section III, the capability of the interaction model used by EURIDICE to correctly simulate the excitation of parasitic backward waves is discussed, and EURIDICE results are compared to results by simpleRick. Section IV summarizes the findings of this article.

II. SIMULATION OF PARASITIC EXCITATION OF BACKWARD WAVES

The beam–wave interaction in the cavity of the 1-MW 140-GHz $TE_{28,8}$ -mode gyrotron and in the cavity of the 1.5-MW 140-GHz $TE_{28,10}$ -mode gyrotron was simulated with EURIDICE, assuming operating parameters close to nominal. The simulation domain was the three-section cavity (downtaper–midsection–uptaper) plus the conical metallic spacer connecting the cavity to the beam tunnel. The inclusion of the spacer had the purpose to address the possible penetration/interaction of the backward waves in that region, since they travel opposite to the direction of the electron beam. The number of TE modes included in the multimode simulations was greatly increased, in order to consider modes with resonant frequencies as low as 25% below the nominal frequency. This is opposed to the usual practice, where competing modes only in the region $\pm 5\%$ of the nominal frequency are included in the simulation [10]. Several values for the electron velocity ratio α were considered, including the nominal as well as lower and higher values.

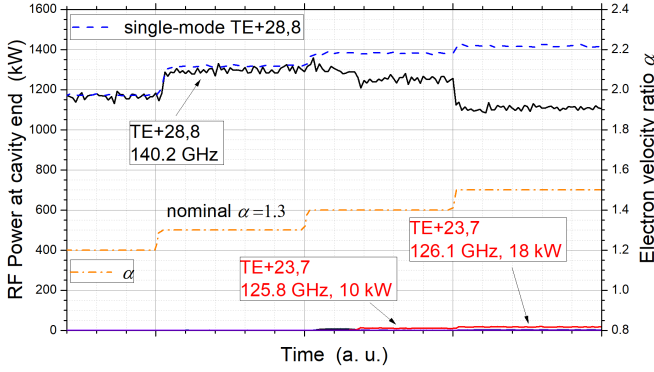


Fig. 1. Multimode simulation (EURIDICE; 161 modes) of the operation of the 1-MW 140-GHz $TE_{28,8}$ -mode gyrotron at parameters close to nominal (see text), considering four different values of the electron velocity ratio. RF power at the cavity exit (solid curves) and electron velocity ratio (dashed-dotted orange curve) is shown. The parasitic excitation of the $TE_{23,7}$ mode at $\alpha = 1.4$ and 1.5 as a backward wave results in significant power loss for the operating mode, as compared to the single-mode simulation ignoring the competing modes (dashed blue curve).

A. Results With Nominal Velocity Spread

The simulation results for the 1-MW 140-GHz gyrotron [12] are shown in Fig. 1. Operation close to nominal was considered, with electron energy $E_{kin} = 78$ keV, beam current $I_b = 46$ A, magnetic field at the cavity $B_0 = 5.56$ T, and electron beam radius $R_b = 10.1$ mm. Four different values of the electron velocity ratio α were simulated, including the nominal value $\alpha = 1.3$. Typical design values of a 3% uniform guiding-center spread and a 5% rms spread in α (corresponding to $\sim 3\%$ spread in perpendicular velocity) were assumed. In total, 161 TE modes (including the nominal operating mode $TE_{28,8}$) were considered, having lowest resonant frequencies in the range 75%–105% of the nominal operating frequency and beam–wave coupling coefficient at least as high as 70% of the coupling coefficient of the $TE_{28,8}$ mode.

As can be seen from Fig. 1, for the nominal electron velocity ratio or lower, there is no parasitic mode excitation, the operation is essentially single mode, and the operating mode achieves the same performance to that predicted by the single-mode simulation considering only the $TE_{28,8}$ mode and ignoring the competing modes (dashed blue curve in Fig. 1). For the higher than nominal values $\alpha = 1.4$ and 1.5 , the parasitic excitation of the $TE_{23,7}$ mode at ~ 126 GHz is observed at low power levels, in the range of 10–20 kW. Despite the low power level, this excitation has a considerable effect on the main interaction of the electron beam with the $TE_{28,8}$ mode leading to a power degradation of 9% and 22% (compared to the single-mode simulation) for $\alpha = 1.4$ and 1.5 , respectively. The parasitic mode is excited as a backward wave, since its oscillating frequency is lower than the electron cyclotron frequency. This is shown in Table I, where all the characteristic frequencies of the 1-MW 140-GHz gyrotron are given. Also, as can be seen from the table, the dependence of the oscillating frequency of the parasitic mode on the operating parameters (here, the value of α) is stronger than that of the oscillating frequency of the operating mode. This

TABLE I
CHARACTERISTIC FREQUENCIES (GHz) OF THE
1-MW 140-GHz GYROTRON

	Nominal mode $TE_{28,8}$	Parasitic mode $TE_{23,7}$
Cyclotron frequency variation along the simulated geometry	132.3 - 135.0	
Cutoff frequency at geometry input / midsection	197.8 / 140.0	165.9 / 117.4
Lowest resonant frequency in cold cavity (i.e. in the absence of electron beam)	140.2	117.6
Oscillating frequency at $\alpha = 1.4 / \alpha = 1.5$	140.2	125.8 / 126.1

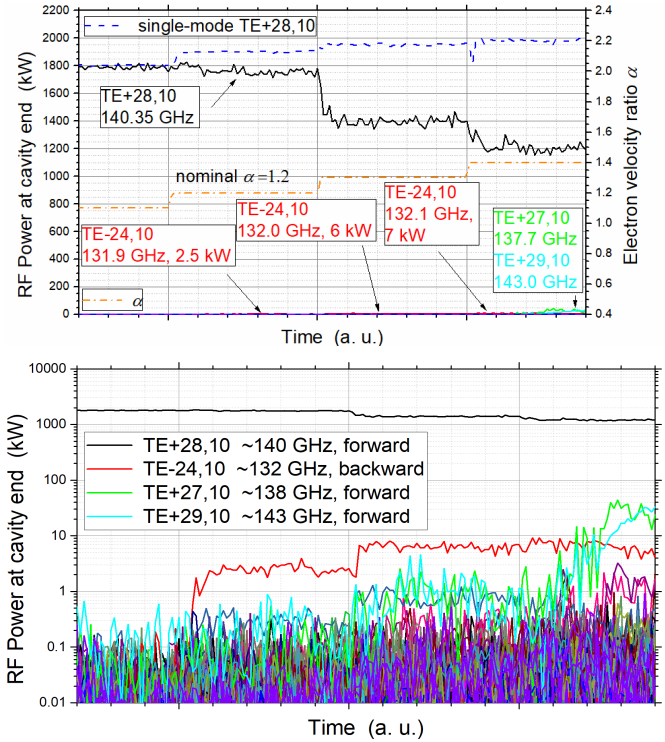


Fig. 2. Top: multimode simulation (EURIDICE; 202 modes) of the operation of the 1.5-MW 140-GHz $TE_{28,10}$ -mode gyrotron at parameters close to nominal (see text), considering four different values of the electron velocity ratio. RF power at the cavity exit (solid curves) and electron velocity ratio (dashed-dotted orange curve) is shown. The parasitic excitation of the counter-rotating mode $TE_{-24,10}$ at $\alpha = 1.2$ – 1.4 as a backward wave results in power loss for the operating mode, as compared to the single-mode simulation that ignores the competing modes (dashed blue curve). Bottom: the same in logarithmic scale.

is a characteristic difference in the behavior of a backward and a forward wave.

Similar findings appeared in the simulation of the 1.5-MW 140-GHz gyrotron [13], which are shown in Fig. 2. Again, operation close to nominal was considered ($E_{kin} = 80$ keV, $I_b = 55$ A, $B_0 = 5.56$ T, and $R_b = 10.1$ mm) with four different values of the electron velocity ratio, including the nominal value $\alpha = 1.2$. Typical design values of a 3.6% uniform guiding-center spread and a 5% rms spread in α were assumed. In total, 202 TE modes (including the nominal mode $TE_{28,10}$) were considered. Their resonant frequencies were in

TABLE II
CHARACTERISTIC FREQUENCIES (GHz) OF THE
1.5-MW 140-GHz GYROTRON

	Nominal mode TE _{28,10}	Parasitic mode TE _{-24,10}
Cyclotron frequency variation along the simulated geometry	131.9 - 134.6	
Cutoff frequency at geometry input / midsection	217.8 / 140.2	201.4 / 129.7
Lowest resonant frequency in cold cavity (i.e. in the absence of electron beam)	140.35	129.8
Oscillating frequency at $\alpha = 1.2 / \alpha = 1.3 / \alpha = 1.4$	140.36	131.9 / 132.0 / 132.1

the range 75%–105% of the nominal operating frequency and their beam–wave coupling coefficient was at least as high as 75% of the coupling coefficient of the TE_{28,10} mode.

According to Fig. 2, at $\alpha = 1.1$, there is no parasitic excitation and the operation is essentially single-mode in the TE_{28,10} mode. However, even at the nominal value $\alpha = 1.2$, the excitation of the counter-rotating TE_{-24,10} mode at 131.9 GHz with a power as low as 2.5 kW results in an 8% power reduction in the operating mode. From Table II, it is clear that the TE_{-24,10} mode is excited as a backward wave, with a frequency lower than the electron cyclotron frequency. At the higher values $\alpha = 1.3$ and 1.4, the excitation of the TE_{-24,10} mode persists at increased power (6–7 kW) and results in severe power reduction of the operating mode, in the order of 29% and 39%, respectively, as compared to the single-mode calculation (dashed blue curve). At these higher α -values, there is also parasitic excitation of the usual azimuthal satellite modes TE_{27,10} and TE_{29,10} of the nominal mode (forward waves—three-wave effect). As already mentioned in Section I, the frequency of the lower satellite mode TE_{27,10} is only 2% lower than the nominal frequency.

It is worth mentioning that the above results are in line with experimental findings. As reported in [10], [22], and [23], in order to avoid parasitic signals and obtain optimum performance during the experimental testing of the 1.5-MW 140-GHz gyrotron, values of α below 1.2 had to be used. Indeed, according to Fig. 2, the parasitic excitation in this gyrotron takes place at $\alpha \geq 1.2$. Moreover, the experimentally measured parasitic frequencies in the 1.5-MW gyrotron, reported in [10], were in the range 130–134 GHz. This is in line with the simulations in [10], which predicted backward-wave parasitics at relevant frequencies, namely, at 127.9 and 130.9 GHz. Also, with respect to the 1.0-MW 140-GHz gyrotron, the parasitic frequencies during experiments appeared in the range 120–130 GHz [4]. In the simulation of nominal operation of the 1.0-MW gyrotron shown in Fig. 1, a backward-wave parasitic at ~ 126 GHz is excited. Thus, the relevance of the simulated parasitic frequencies to the experimental findings with the two gyrotrons strengthens the possibility that the excitation of backward waves in the cavity could be the origin of experimentally measured parasitic frequencies, along with the beam-tunnel parasitics or the after-cavity interaction.

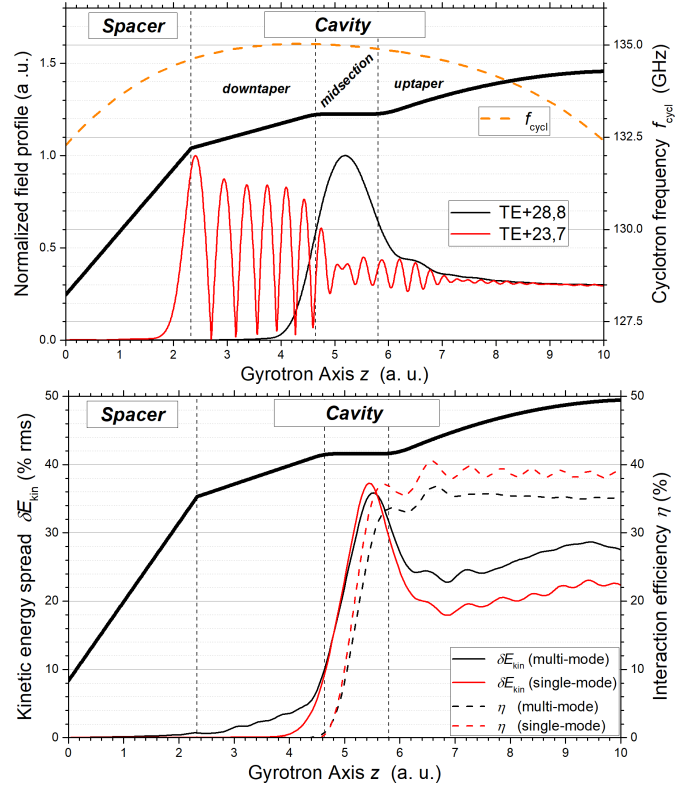


Fig. 3. Results for the case of Fig. 1 at $\alpha = 1.4$. The contour of the simulated geometry with midsection radius 20.48 mm and midsection length 14.5 mm is shown by the thick black curve. Top: RF field amplitude, normalized to unity, of the nominal and the parasitic mode along the gyrotron axis. The electron cyclotron frequency, prior to interaction, is also shown (dashed curve). Bottom: rms spread of the electron kinetic energy and interaction efficiency along the gyrotron axis, calculated by multimode and single-mode simulation. The high energy spread ($\sim 2.5\%$), induced by the parasitic backward-wave mode at $z \sim 3.5$, is decreasing the efficiency of the main interaction by 3.5 percentage units, as compared to the single-mode result.

B. Underlying Mechanism of Power Decrease

The mechanism by which the parasitic backward-wave excitation, although at low power levels, significantly affects the beam–wave interaction of the nominal mode is illustrated in Fig. 3. The figure refers to the case of the 1-MW 140-GHz TE_{28,8}-mode gyrotron, simulated with $\alpha = 1.4$ (see Fig. 1). In Fig. 3(top), the amplitude of the RF field profile of the nominal TE_{28,8} mode and of the parasitic TE_{23,7} mode are shown, together with the contour of the simulated geometry (spacer and three-section cavity; arbitrary units). Both field profiles are normalized to unity. The parasitic backward TE_{23,7} wave is excited at a frequency noticeably higher than its cutoff frequency at the cavity midsection (see Table I), which permits the field penetration into the downtaper and spacer region. At some point in the spacer ($z < 2$), the cutoff is reached, and the backward wave is reflected toward the cavity output. This results in the visible standing-wave pattern. Also, from this pattern, it can be suggested that the backward-wave excitation is not restricted in the downtaper–spacer region but begins already at the cavity midsection. Contrary to the backward-wave mode, the nominal TE_{28,8} mode is excited very close to cutoff at the cavity midsection as a forward wave and its

field penetrates only into half the downtaper ($z \sim 3.5$). This difference in downtaper penetration between the nominal mode and the parasitic mode has the consequence that the interaction of the parasitic backward wave with the electron beam begins well before the interaction of the beam with the nominal mode. This early interaction of the parasitic mode induces energy spread to the electrons, and when the interaction of the nominal mode starts (at $z \sim 3.5$), this energy spread is already very high and results in poorer main interaction. This is clear in Fig. 3(bottom), where the kinetic energy spread and the efficiency of the beam–wave interaction are plotted along the gyrotron axis. The parasitic backward wave induces a $\sim 2.5\%$ rms energy spread at $z \sim 3.5$ and this results in a decreased efficiency of the main interaction by 9% (3.5 percentage units), as compared to the single-mode simulation, which ignores the parasitic mode. It is remarkable that a parasitic excitation with power as low as ~ 10 kW (i.e., $< 1\%$ of the power of the nominal mode, see Fig. 1) can have such a significant effect, and this is explained by the induced energy spread. It is also interesting to note that the typical design values of the energy spread in the two simulated gyrotrons are as low as 0.01%–0.1% rms.

C. Results With Increased Velocity Spread

As can be seen from Tables I and II, the parasitic backward wave is oscillating in the midsection at a frequency that is $\sim 7\%$ or $\sim 2\%$ higher than its cutoff frequency, for the TE_{28,8}-mode gyrotron or the TE_{28,10}-mode gyrotron, respectively. The oscillating frequency of the operating mode is only $\sim 0.1\%$ higher than the cutoff frequency in both gyrotrons. This means that the excitation of the parasitic backward waves is much more Doppler-shifted than that of the operating mode, and this is also visible in Fig. 3(top). Consequently, the electron velocity spread is expected to influence the parasitic excitation much more than the nominal excitation, as was also shown in [14]. To study this, the simulations of Figs. 1 and 2 were repeated assuming increased values of the spreads in the electron velocity ratio.

The results are shown in Figs. 4 and 5 and confirm the above expectation. In the case of the 1-MW 140-GHz gyrotron, if the rms spread in the electron velocity ratio α is increased to $\delta\alpha = 10\%$ rms (equivalent to $\delta v_{\perp} \cong 6\%–7\%$), the parasitic mode excitation is happening only at $\alpha = 1.5$ and is much less pronounced. With $\delta\alpha = 20\%$ rms (equivalent to $\delta v_{\perp} \cong 12\%–14\%$), there is no parasitic excitation of backward waves. As expected, the increased velocity spread reduces the efficiency of the main interaction too, as can be seen from the single-mode simulations at the different values of the velocity spread. In the case of the 1.5-MW 140-GHz gyrotron, the parasitic mode excitation is again impeded by increasing velocity spread and appears only at the values of α higher than nominal (Fig. 5).

The weakening of the excitation of parasitic backward waves by the increase of the velocity spread suggests the following two points: first, since the velocity spread in experiments is expected to be higher than the design value, the parasitic mode excitation would, in reality, be less severe than

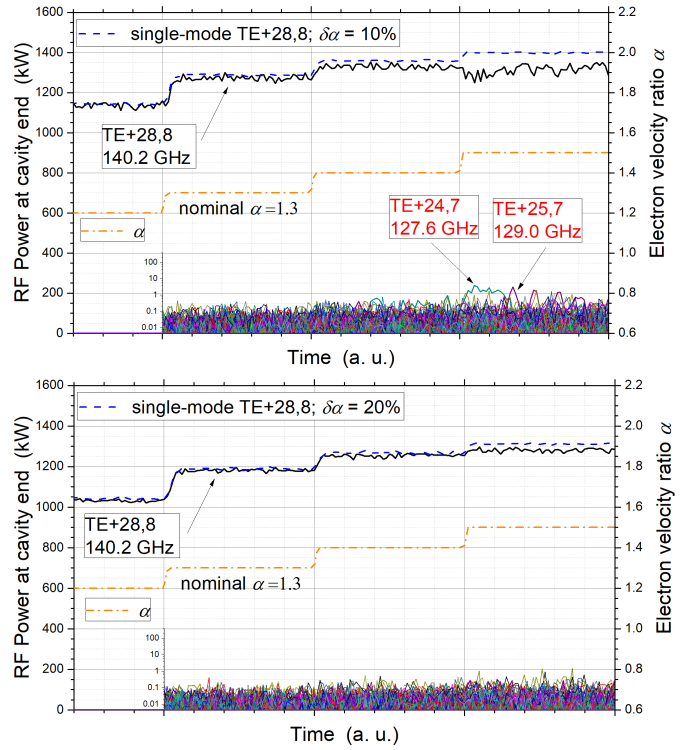


Fig. 4. Multimode simulation of the operation of the 1-MW 140-GHz TE_{28,8}-mode gyrotron at parameters identical to those of Fig. 1 but with increased velocity spread $\delta\alpha = 10\%$ rms (top) and $\delta\alpha = 20\%$ rms (bottom). The power of the competing modes is shown in logarithmic scale at the insets. The result of single-mode simulation ignoring competing modes is shown by the dashed blue curve. The parasitic backward-wave excitation is practically suppressed by the increased velocity spread, except for the case $\alpha = 1.5$ and $\delta\alpha = 10\%$ rms, where some weak excitation of the modes TE_{24,7} and TE_{25,7} takes place.

what is predicted in Figs. 1 and 2. Second, a reasonable increase, by design, of the velocity spread may be beneficial with respect to the suppression of backward-wave excitation. Such a practice has also been proposed in [24], albeit within a different context relevant to a low-power 1.2-THz third-harmonic gyrotron.

III. DISCUSSION ON MODELING AND VALIDATION

A. Key Points for Correct Modeling/Simulation

There is a list of points where the correct modeling and simulation of the parasitic backward-wave excitation is challenging, requiring advances with respect to the standard models and practices used in gyrotron interaction simulations. These points are given in the following, accompanied by a discussion on whether EURIDICE complies with the associated requirements.

1) The simulations are computationally much more demanding than the standard multimode interaction simulations of the gyrotron cavity. This is because of three reasons: (a) to capture the parasitic modes that are excited as backward waves, TE modes with a very low resonant frequency in the cold cavity need to be considered. That is, the cold-cavity frequency of the competing modes should not be restricted to the usual range of about $\pm 5\%$ of the operating frequency (gyrotron resonance band) but should extend to much lower values. This

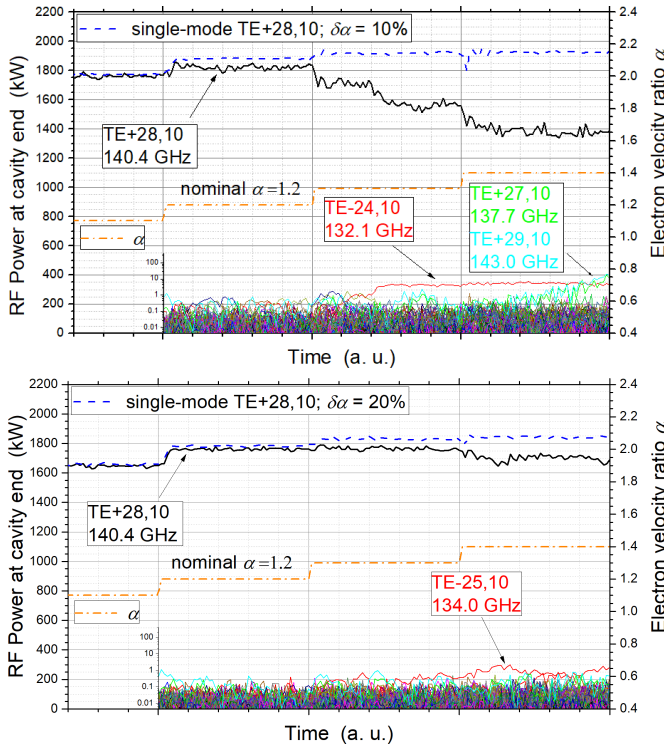


Fig. 5. Multimode simulation of the operation of the 1.5-MW 140-GHz $TE_{28,10}$ -mode gyrotron at parameters identical to those of Fig. 2 but with increased velocity spread $\delta\alpha = 10\%$ rms (top) and $\delta\alpha = 20\%$ rms (bottom). The power of the competing modes is shown in logarithmic scale in the insets. The result of single-mode simulation ignoring competing modes is shown by the dashed blue curve. The parasitic backward-wave excitation is decreasing by increasing velocity spread.

leads to a large increase of the number of competing modes. (Indicatively, for the simulations in this article, the number of competing modes was increased from ~ 60 – 80 to ~ 150 – 200 .) (b) Clearly, the spacer region should also be considered in the simulations because of the penetration of the backward waves, and this lengthens noticeably the simulated geometry. (c) The Doppler-shifted nature of the backward-wave excitation results in a field profile with faster spatial variation along the gyrotron axis [see Fig. 3(top)], necessitating an adequately fine axial discretization.

2) The forward-wave gyrotron modes are excited very close to cutoff, and the influence of the transverse RF magnetic field on the beam–wave interaction can be neglected, as this field vanishes at cutoff. This is usually done in standard gyrotron interaction modeling (e.g., [18], [25]), and as also discussed in [26], it is a well-justified approximation. However, the backward-wave modes under investigation are excited farther from cutoff. Consequently, the transverse RF magnetic field should not, in principle, be neglected and therefore, it is included in EURIDICE simulations. (It may also be noted that the transverse RF magnetic field can sometimes be significant also for modes excited close to cutoff: this is the case when giant ultrashort pulses in gyrotrons are considered [27].)

3) In the slow-variables approach, the electric field of a TE_n mode is represented as $\mathbf{E} = \text{Re}\{A(z, t) \mathbf{e}_n e^{i\omega t}\}$ [18], where \mathbf{e}_n is the transverse eigenvector, $A(z, t)$ is the complex

field profile along the cavity axis z , and ω is a carrier frequency, which is arbitrarily chosen, but which has to be close to the actual oscillating frequency of the mode. The usual trajectory approach for the electron motion assumes that the profile $A(z, t)$ remains unchanged during the electron transit time. Consequently, the closer the carrier ω is to the actual frequency, the more accurate is the slow-variables trajectory model. In the standard gyrotron interaction with forward waves, ω is usually chosen to be the cold-cavity frequency or the cutoff frequency, and both choices are suitable because the actual frequency of the mode is not much different than those frequencies. However, this is not the case for the backward waves, whose oscillating frequencies are quite far from the cutoff or the cold-cavity frequency. All the above are apparent in Tables I and II. Consequently, the correct choice of the carrier ω for the backward waves is not obvious prior to their excitation, and this strongly impairs the validity of the model. Nevertheless, EURIDICE overcomes this shortcoming because it uses the advanced concept of a varying carrier frequency [20], which is slowly adjusting to the actual frequency during the simulation. In particular, at each time step, the frequency of the mode is calculated, and the carrier frequency is set equal to the average frequency of the mode over several previous time steps. At this point, it should also be noted that if the PIC approach is used for the electron motion, the choice of the carrier is not so important because, contrary to the trajectory approach, the RF field envelope $A(z, t)$ is updated many times during the electron transit.

4) In the standard gyrotron interaction model, it is very expedient to use the Graf addition theorem and perform gyro-averaging (e.g., [25]). The infinite Graf’s sum over k contains terms with a time dependence $\sim \exp[i(\omega - k\omega_{\text{cycl}})t]$, where ω is the carrier frequency of the mode and ω_{cycl} is the electron cyclotron frequency. After gyro-averaging, only one term is kept, in particular the term with $k = s$, where s is the harmonic number of interaction of the mode. This is done on the grounds that the gyrotron resonance condition $\omega \cong s\omega_{\text{cycl}}$ holds true for the mode. In the case of forward waves, the difference between ω and $s\omega_{\text{cycl}}$ is of the order of 3%–4% because of the very small Doppler shift (see also Tables I and II; $s = 1$ for interaction at the fundamental cyclotron frequency). On the other hand, in the case of backward waves, the Doppler shift is increased and the difference between ω and $s\omega_{\text{cycl}}$ can, in general, be larger. For instance, in Table I, this difference can reach 7%, if a carrier frequency close to the actual oscillating frequency is chosen, as discussed in point (3). In conclusion, there can be, in principle, cases of parasitic backward-wave excitation, where gyro-averaging and the subsequent reduction of the Graf’s sum to only one term could introduce some error.

5) With the inclusion of the spacer region, the length of the simulation domain increases and a question may arise on whether the amplitude $|A(z, t)|$ remains constant during the electron transit, which is a prerequisite for the validity of the trajectory approach. Therefore, a PIC simulation or, alternatively, the use of an advanced interaction model that takes into account the change of the RF field amplitude during

TABLE III
TWO-MODE SIMULATION OF THE 1-MW 140-GHz GYROTRON
RESULTS BY EURIDICE/SIMPLERICK

α	Power [kW]		Frequency [GHz]	
	TE _{28,8}	TE _{23,7}	TE _{28,8}	TE _{23,7}
1.3	1308 / 1274	0 / 0	140.2 / 140.2	- / -
1.4	1280 / 1033	8 / 10	140.2 / 140.2	125.9 / 125.7
1.5	1151 / 1078	14 / 15	140.2 / 140.2	126.1 / 126.0

TABLE IV
TWO-MODE SIMULATION OF THE 1.5-MW 140-GHz GYROTRON
RESULTS BY EURIDICE/SIMPLERICK

α	Power [kW]		Frequency [GHz]	
	TE _{28,10}	TE _{-24,10}	TE _{28,10}	TE _{-24,10}
1.2	1817 / 1824	2 / 2	140.4 / 140.3	131.9 / 131.9
1.3	1384 / 1498	7 / 6	140.4 / 140.3	132.0 / 131.9
1.4	1152 / 1309	8 / 8	140.4 / 140.3	132.1 / 132.1

the electron transit [28], [29], appears advantageous in that respect.

B. Comparison of Codes and Validation of the Results

As is apparent from the previous discussion, the presented simulations by EURIDICE comply with points (1)–(3) but not with points (4) and (5). This could lead to less accurate modeling of the backward-wave excitation. To validate EURIDICE results, a direct comparison with the code simpleRick was performed. simpleRick complies with all points (1)–(5), because it is a PIC code and is using the slow-variables approach without gyro-averaging of the electron motion. However, because of the increased modeling accuracy, multimode simulations with simpleRick become computationally demanding as the number of competing modes increases. To secure a direct comparison, the simulations of Figs. 1 and 2 were repeated by EURIDICE using only two modes, i.e., the operating mode and the excited parasitic mode, and were compared to the same two-mode simulations by simpleRick.

The results are shown in Tables III and IV. The codes are in excellent agreement as far as the frequency is concerned, with a maximum discrepancy below 0.2%. With respect to the power of the operating mode and the parasitic mode, the maximum discrepancy between the codes is of the order of 20%. The following conclusions can be drawn from this comparison: (1) despite major differences in the employed models, both codes predict the parasitic mode excitation at the same frequency. (2) The up to ~20% difference in the calculated power shows that, indeed, the modeling can have a nonnegligible quantitative effect. However, the parasitic mode excitation and the associated power reduction of the main mode are qualitatively identical in both codes. This strongly testifies in favor of the parasitic backward-wave excitation being a real physical effect.

IV. SUMMARY

The possibility of parasitic RF excitation of backward-wave modes in high-power gyrotron cavities was demonstrated for two existing gyrotrons by multimode simulations using two different codes. The parasitic excitation can lead to a significant performance degradation of the nominal operating mode: even at power levels below 1% of the nominal power, the parasitic mode results in a power reduction of the order of 10%. The cause of the performance degradation was identified to be the increased energy spread in the downtaper and spacer region. This spread is induced by the parasitic mode, which, contrary to the nominal mode, is capable of propagating in this region and thus impacts the electron beam prior to its interaction with the nominal mode. In the simulated cases, the parasitic backward-wave excitation strengthens with increasing values of the electron velocity ratio α but weakens with increasing velocity spread, being a Doppler-shifted excitation.

The validity of the employed models for the interaction of the electron beam with the RF wave, with respect to their ability to accurately simulate the parasitic backward-wave excitation, was discussed in detail. A comparison of the results of EURIDICE (trajectory code using gyro-averaging) and simpleRick (PIC code without gyro-averaging of the electron motion) showed excellent qualitative agreement, excellent quantitative agreement in the frequency calculation (<0.2% difference), and reasonable quantitative agreement in the power calculation (~20% maximum difference). Based on those findings, it can be proposed that the parasitic backward-wave excitation is a possible physical effect. It can be an additional source of origin, besides the parasitic mode excitation in the gyrotron beam tunnel or after the gyrotron cavity, of the parasitic RF frequencies in the range 5%–15% below the nominal frequency, observed experimentally in high-power gyrotrons, operating in high-order modes.

Further steps in the investigations on parasitic backward waves in gyrotron cavities will include comprehensive studies on their dependence on the various physical and numerical parameters, in order first to optimize the modeling tools and second to examine the possible ways of suppression of the parasitic excitation. In addition, the particularities of the excited backward-wave modes, with respect to beam-wave coupling, magnitude of Doppler term, and frequency detuning, will be studied, attempting to identify the reasons why one parasitic mode is favored over another.

ACKNOWLEDGMENT

Part of the simulations was performed on the EUROfusion High Performance Computer (Marconi-Fusion).

REFERENCES

- [1] I. I. Antakov, I. G. Gachev, and E. V. Zasyupkin, "Self-excitation of spurious oscillations in the drift region of gyrotrons and their influence on gyrotron operation," *IEEE Trans. Plasma Sci.*, vol. 22, no. 5, pp. 878–882, Oct. 1994, doi: 10.1109/27.338303.

- [2] M. Pedrozzi, S. Alberti, J. P. Hogge, M. Q. Tran, and T. M. Tran, "Electron beam instabilities in gyrotron beam tunnels," *Phys. Plasmas*, vol. 5, no. 6, pp. 2421–2430, Jun. 1998, doi: [10.1063/1.872918](https://doi.org/10.1063/1.872918).
- [3] K. Sakamoto et al., "Development of 170 and 110 GHz gyrotrons for fusion devices," *Nucl. Fusion*, vol. 43, no. 8, pp. 729–737, Aug. 2003, doi: [10.1088/0029-5515/43/8/314](https://doi.org/10.1088/0029-5515/43/8/314).
- [4] G. Gantenbein et al., "Experimental investigations and analysis of parasitic RF oscillations in high-power gyrotrons," *IEEE Trans. Plasma Sci.*, vol. 38, no. 6, pp. 1168–1177, Jun. 2010, doi: [10.1109/TPS.2010.2041366](https://doi.org/10.1109/TPS.2010.2041366).
- [5] Z. C. Ioannidis, I. Chelis, G. Gantenbein, T. Rzesnicki, and J. Jelonek, "Experimental classification and enhanced suppression of parasitic oscillations in gyrotron beam tunnels," *IEEE Trans. Electron Devices*, vol. 67, no. 12, pp. 5783–5789, Dec. 2020, doi: [10.1109/TED.2020.3025751](https://doi.org/10.1109/TED.2020.3025751).
- [6] S. Kern et al., "Simulation and experimental investigations on dynamic after cavity interaction (ACI)," in *Proc. 35th Int. Conf. Infr., Millim., Terahertz Waves*, Sep. 2010, pp. 5–10, doi: [10.1109/ICIMW.2010.5612609](https://doi.org/10.1109/ICIMW.2010.5612609).
- [7] A. Schlaich et al., "Examination of parasitic after-cavity oscillations in the W7-X series gyrotron SN4R," in *Proc. Int. Conf. Infr., Millim., Terahertz Waves*, Houston, TX, USA, Oct. 2011, pp. 2–7, doi: [10.1109/irmmw-THz.2011.6104902](https://doi.org/10.1109/irmmw-THz.2011.6104902).
- [8] K. A. Avramidis et al., "A comparative study on the modeling of dynamic after-cavity interaction in gyrotrons," *Phys. Plasmas*, vol. 22, no. 5, May 2015, Art. no. 053106, doi: [10.1063/1.4919924](https://doi.org/10.1063/1.4919924).
- [9] A. R. Choudhury, D. D'Andrea, and M. Thumm, "Study of dynamic after cavity interaction in gyrotrons—Part II: Influence of a nonuniform magnetic field," *IEEE Trans. Electron Devices*, vol. 62, no. 1, pp. 192–199, Jan. 2015, doi: [10.1109/TED.2014.2367314](https://doi.org/10.1109/TED.2014.2367314).
- [10] K. A. Avramidis et al., "Multifaceted simulations reproducing experimental results from the 1.5-MW 140-GHz preprototype gyrotron for W7-X," *IEEE Trans. Electron Devices*, vol. 68, no. 6, pp. 3063–3069, Jun. 2021, doi: [10.1109/TED.2021.3075653](https://doi.org/10.1109/TED.2021.3075653).
- [11] M. H. Beringer, S. Kern, and M. Thumm, "Mode selection and coaxial cavity design for a 4-MW 170-GHz gyrotron, including thermal aspects," *IEEE Trans. Plasma Sci.*, vol. 41, no. 4, pp. 853–861, Apr. 2013, doi: [10.1109/TPS.2013.2251870](https://doi.org/10.1109/TPS.2013.2251870).
- [12] M. Thumm et al., "Progress in the 10-MW 140-GHz ECH system for the stellarator W7-X," *IEEE Trans. Plasma Sci.*, vol. 36, no. 2, pp. 341–355, Apr. 2008, doi: [10.1109/TPS.2008.917950](https://doi.org/10.1109/TPS.2008.917950).
- [13] K. A. Avramidis et al., "Towards a 1.5 MW, 140 GHz gyrotron for the upgraded ECRH system at W7-X," *Fusion Eng. Des.*, vol. 164, Mar. 2021, Art. no. 112173, doi: [10.1016/j.fusengdes.2020.112173](https://doi.org/10.1016/j.fusengdes.2020.112173).
- [14] J. Genoud et al., "Parasitic oscillations in smooth-wall circular symmetric gyrotron beam ducts," *J. Infr., Millim., Terahertz Waves*, vol. 40, no. 2, pp. 131–149, Oct. 2018, doi: [10.1007/s10762-018-0548-5](https://doi.org/10.1007/s10762-018-0548-5).
- [15] A. W. Fliflet, R. C. Lee, S. H. Gold, W. M. Manheimer, and E. Ott, "Time-dependent multimode simulation of gyrotron oscillators," *Phys. Rev. A, Gen. Phys.*, vol. 43, pp. 6166–6176, Nov. 1991, doi: [10.1103/PhysRevA.43.6166](https://doi.org/10.1103/PhysRevA.43.6166).
- [16] S. H. Gold and A. W. Fliflet, "Multimode simulation of high frequency gyrotrons," *Int. J. Electron.*, vol. 72, nos. 5–6, pp. 779–794, May 1992, doi: [10.1080/00207219208925614](https://doi.org/10.1080/00207219208925614).
- [17] S. P. Sabchevski, M. Y. Glyavin, and G. S. Nusinovich, "The progress in the studies of mode interaction in gyrotrons," *J. Infr., Millim., Terahertz Waves*, vol. 43, nos. 1–2, pp. 1–47, Mar. 2022, doi: [10.1007/s10762-022-00845-7](https://doi.org/10.1007/s10762-022-00845-7).
- [18] N. S. Ginzburg, G. S. Nusinovich, and N. A. Zavolsky, "Theory of non-stationary processes in gyrotrons with low Q resonators," *Int. J. Electron.*, vol. 61, pp. 881–894, Nov. 1986, doi: [10.1080/00207218608920927](https://doi.org/10.1080/00207218608920927).
- [19] K. A. Avramides, I. G. Pagonakis, C. T. Iatrou, and J. L. Vomvouridis, "EURIDICE: A code-package for gyrotron interaction simulations and cavity design," in *Proc. EPJ Web Conf.*, vol. 32, Sep. 2012, p. 04016, doi: [10.1051/epjconf/20123204016](https://doi.org/10.1051/epjconf/20123204016).
- [20] K. A. Avramidis, "Investigations and advanced concepts on gyrotron interaction modeling and simulations," *Phys. Plasmas*, vol. 22, no. 12, Dec. 2015, Art. no. 123114, doi: [10.1063/1.4938043](https://doi.org/10.1063/1.4938043).
- [21] J. Marek et al., "Time-domain simulation of helical gyro-TWTs with coupled modes method and 3-D particle beam," *IEEE Trans. Electron Devices*, vol. 69, no. 8, pp. 4546–4552, Aug. 2022, doi: [10.1109/TED.2022.3182292](https://doi.org/10.1109/TED.2022.3182292).
- [22] Z. C. Ioannidis et al., "Generation of 1.5 MW–140 GHz pulses with the modular pre-prototype gyrotron for W7-X," *IEEE Electron Device Lett.*, vol. 42, no. 6, pp. 939–942, Jun. 2021, doi: [10.1109/LED.2021.3073221](https://doi.org/10.1109/LED.2021.3073221).
- [23] K. Avramidis, T. Rzesnicki, Z. Ioannidis, and L. Krier, "2021-W7X-3.3.2-KIT: Report on 1.5 MW gyrotron tests and developments," EUROfusion, Garching, Germany, Tech. Rep., W7X-3.3.2-T005-D001, Nov. 2021. [Online]. Available: <https://idm.euro-fusion.org/default.aspx?uid=2PFWAW>
- [24] I. Bandurkin et al., "Development of third-harmonic 1.2-THz gyrotron with intentionally increased velocity spread of electrons," *IEEE Trans. Electron Devices*, vol. 67, no. 10, pp. 4432–4436, Oct. 2020, doi: [10.1109/TED.2020.3012524](https://doi.org/10.1109/TED.2020.3012524).
- [25] A. W. Fliflet, M. E. Read, K. R. Chu, and R. Seeley, "A self-consistent field theory for gyrotron oscillators: Application to a low Q gyromonotron," *Int. J. Electron.*, vol. 53, no. 6, pp. 505–521, 1982, doi: [10.1080/00207218208901545](https://doi.org/10.1080/00207218208901545).
- [26] K. A. Avramides and I. G. Pagonakis, "On the effect of the approximations used in gyrotron interaction calculations," in *Proc. 34th Int. Conf. Infr., Millim., Terahertz Waves*, Busan, (South) Korea, Sep. 2009, pp. 21–25, doi: [10.1109/ICIMW.2009.5324768](https://doi.org/10.1109/ICIMW.2009.5324768).
- [27] N. S. Ginzburg, R. M. Rozental, A. S. Sergeev, A. E. Fedotov, I. V. Zotova, and V. P. Tarakanov, "Generation of rogue waves in gyrotrons operating in the regime of developed turbulence," *Phys. Rev. Lett.*, vol. 119, no. 3, Jul. 2017, Art. no. 034801, doi: [10.1103/PhysRevLett.119.034801](https://doi.org/10.1103/PhysRevLett.119.034801).
- [28] N. S. Ginzburg, A. S. Sergeev, I. V. Zotova, and I. V. Zheleznev, "Time-domain theory of gyrotron traveling wave amplifiers operating at grazing incidence," *Phys. Plasmas*, vol. 22, no. 1, Jan. 2015, Art. no. 013112, doi: [10.1063/1.4906364](https://doi.org/10.1063/1.4906364).
- [29] O. Dumbrajs and H. Kalis, "Nonstationary oscillations in gyrotrons revisited," *Phys. Plasmas*, vol. 22, no. 5, May 2015, Art. no. 053113, doi: [10.1063/1.4921665](https://doi.org/10.1063/1.4921665).